ESA CONTRACT REPORT

Contract Report to the European Space Agency

Demonstration of monitoring

August 2010

Authors: S. Di Michele and P. Bauer

WP-3300 report for ESA contract 1-5576/07/NL/CB:
Project QuARL - Quantitative Assessment of the Operational Value of Space-Borne Radar and Lidar Measurements of Cloud and Aerosol Profiles

European Centre for Medium-Range Weather Forecasts
Europäisches Zentrum für mittelfristige Wettervorhersage
Centre européen pour les prévisions météorologiques à moyen terme

ECMWF

Series: ECMWF - ESA Contract Report

A full list of ECMWF Publications can be found on our web site under:
http://www.ecmwf.int/publications/

Contact: library@ecmwf.int

European Centre for Medium-Range Weather Forecasts
Shinfield Park, Reading, RG2 9AX, England

Contract Report to the European Space Agency

Demonstration of monitoring

Authors: S. Di Michele and P. Bauer

WP-3300 report for ESA contract 1-5576/07/NL/CB:
Project QuARL - Quantitative Assessment of the Operational Value of Space-Borne Radar and Lidar Measurements of Cloud and Aerosol Profiles

European Centre for Medium-Range Weather Forecasts
Shinfield Park, Reading, Berkshire, UK

August 2010

ABSTRACT

A basic framework for monitoring CloudSat observations has been established at ECMWF. Reflectivity obtained from CloudSat has been compared to the one simulated from ECMWF model producing time series of their differences. Instrument anomalies have been then simulated to test if problems with data could be identified in the time series. Results suggest that problems with CloudSat observations can be revealed provided that differences are brought outside their typical range of variation.

Contents

1 Introduction

The monitoring of observational data against model output is an important step before the real assimilation of any observations. Every new observation that is brought into the operational analysis system at the European Centre for Medium-Range Weather Forecasts (ECMWF) is first monitored for a period of time. The monitoring activity helps to identify problems that may be affecting the observations (and/or the model). It also provides a template to understand and to optimally exploit at best the new observations before they become fully active in the analysis system. The monitoring system can track departures, observation errors and bias corrections (if applicable) and produces statistics according to observation type, area and period. The complementary usage of many different observations in the system permits to separate between model issues and issues in the observations, for example, related to instrument deterioration.

In this work, a basic framework is established for monitoring CloudSat data (Stephens *et al.*, 2002) within the ECMWF system. Reflectivity first guess departures are calculated comparing CloudSat observations with the output from the forward operator for reflectivities (ZmVar, Di Michele *et al.*, 2009) applied to short-range forecast fields. The system has been tested with a time series of CloudSat data, also simulating instrument failure in order to demonstrate the value of data monitoring for detecting problems in the observations. Given the complexity and volume of the involved data, the monitoring system is developed as an off-line operation, but it is expected to be easily imported in the operational system for future studies and with focus on the Earth, Clouds, Aerosols and Radiation Explorer (EarthCARE) mission.

2 First guess of radar reflectivity

Observed minus first guess departures are used during the assimilation process not only during the minimization, but also for quality control and bias correction (Auligne and McNally, 2007). In the operational system, first guesses of the observations are generated from short-term forecasts. In this study, we follow a similar setup, sketched in Fig. 2.1, where two 12-hour forecasts are run daily starting at 00 UTC and 12 UTC.

Output quantities, which include temperature, humidity, cloud and precipitation (liquid and solid) are saved every three hours. This study is based on a study period obtained running Cycle 36R1 of the ECMWF model with T511 spectral truncation (corresponding to a 40 km grid resolution) from the 1st to the 20th of June 2008. The approach followed to simulate CloudSat reflectivity starting from these variables is described in the next section.

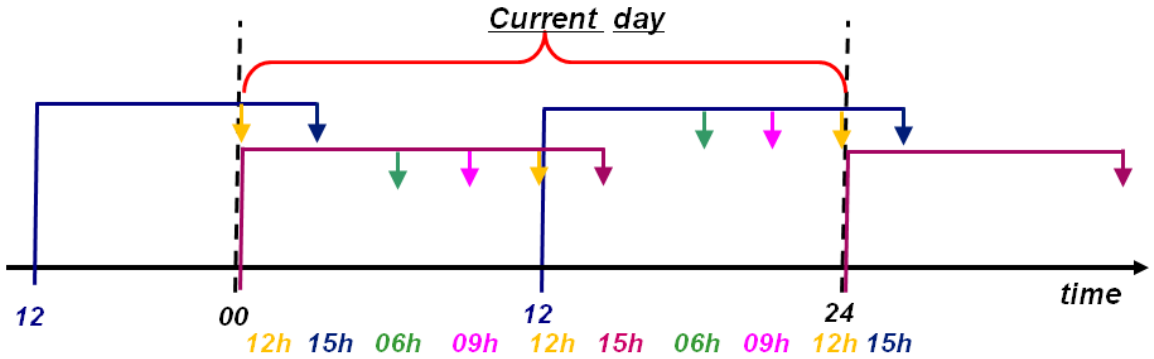

Figure 2.1: *Forecast setup scheme used for generating model first guess.*

2.1 Simulation of cloud radar reflectivity

The first step consists in extracting from the global forecast fields only the model grid-points nearest to CloudSat observations. The selection has been made identifying the closest model profile to each observation, in space and in time.

CloudSat reflectivity for the extracted profiles has been then simulated using the ZmVar radar reflectivity observation operator described in Di Michele *et al.*, 2009. It is worth mentioning that the cloud fraction that the model associates to each profile has been taken into account running ZmVar with the multi-column approach. In this study, a value of 25 for the number of subcolumns has been chosen. Fig. 2.2 shows the reflectivity for a cloud structure observed by CloudSat at high latitudes on the 1st of June 2008 (top panel) and the corresponding one simulated by ZmVar (mid panel). We note how the forecast model is able to realistically reproduce the structure of this event, in spite of slight differences in intensity and location. The contingency mask, shown in Fig. 2.2 (bottom panel), highlights that the model produces cloud fields that are smoother and wider spread.

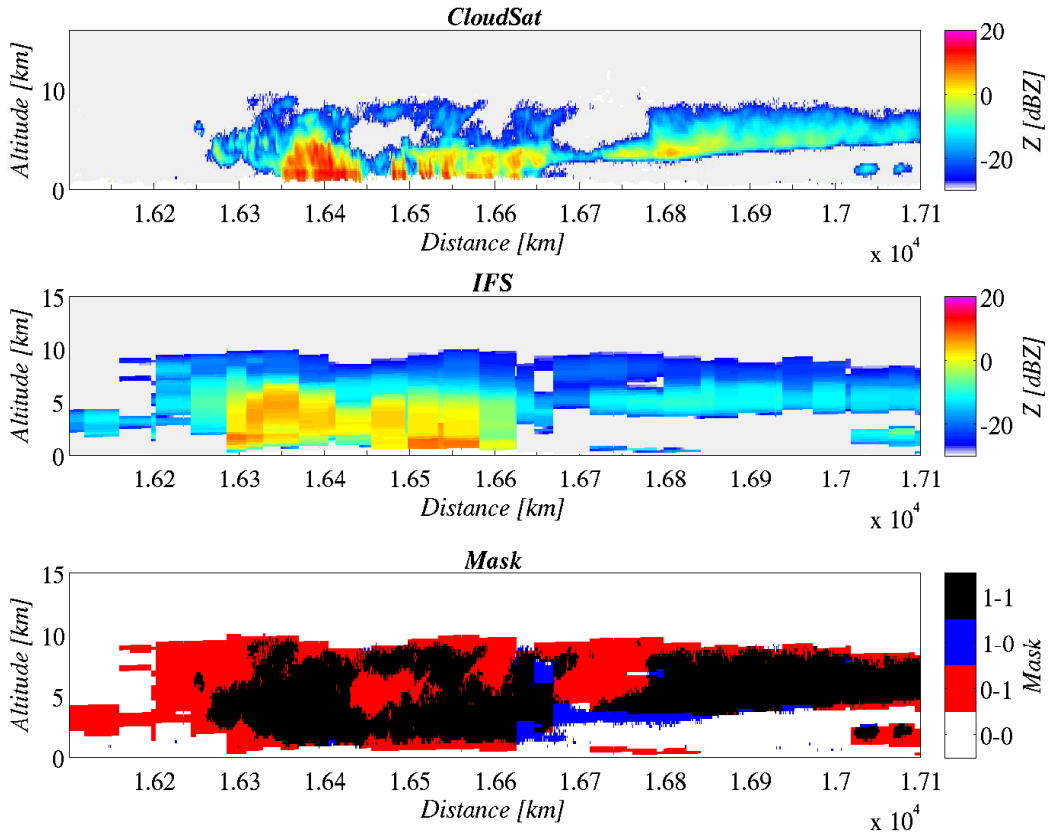

Figure 2.2: *Reflectivity from a high latitude system as observed by CloudSat (top panel), and simulated using the ECMWF forecast model (central panel). Also shown (bottom panel) is the contingency mask between observed and simulated reflectivities.*

3 Comparison of simulated and observed reflectivities

In this section, simulated reflectivity is directly compared with the corresponding CloudSat measurements. This will help in understanding the level of agreement between these two datasets before considering their departures. The model vs. observations comparison has been done using CloudSat data relative to the 20 day period. Only cases over ocean have been considered since the analysis of the reflectivity profiles is facilitated by keeping out the orography. Simulated grid box reflectivity has been evaluated as the mean of the 25 grid-box subcolumns, considering only reflectivity values above the minimum detectable threshold (-27 dBZ for CloudSat). Interesting to note, these reflectivity values are very similar because subcolumns have all the same cloud content and differences can be due only to attenuation from the layers above.

CloudSat has a much higher horizontal resolution than the model (1 km vs. 40 km), and therefore several radar shots fall within each grid box. Fig. 3.1 shows the distribution of CloudSat reflectivity within each model grid-box at three reference heights, considering the case shown in Fig. 2.2. We note that the largest inhomogeneities are at lower levels, at locations where CloudSat crosses the borders of intense structures.

In this study, each CloudSat shot is compared against the closest model reflectivity without any averaging. As noticeable from Fig. 3.1, the distributions of reflectivity in each box are very often asymmetrical. Therefore, if using averaged observations, statistics of differences with model reflectivity would be different, maybe harming the process of monitoring the quality of data.

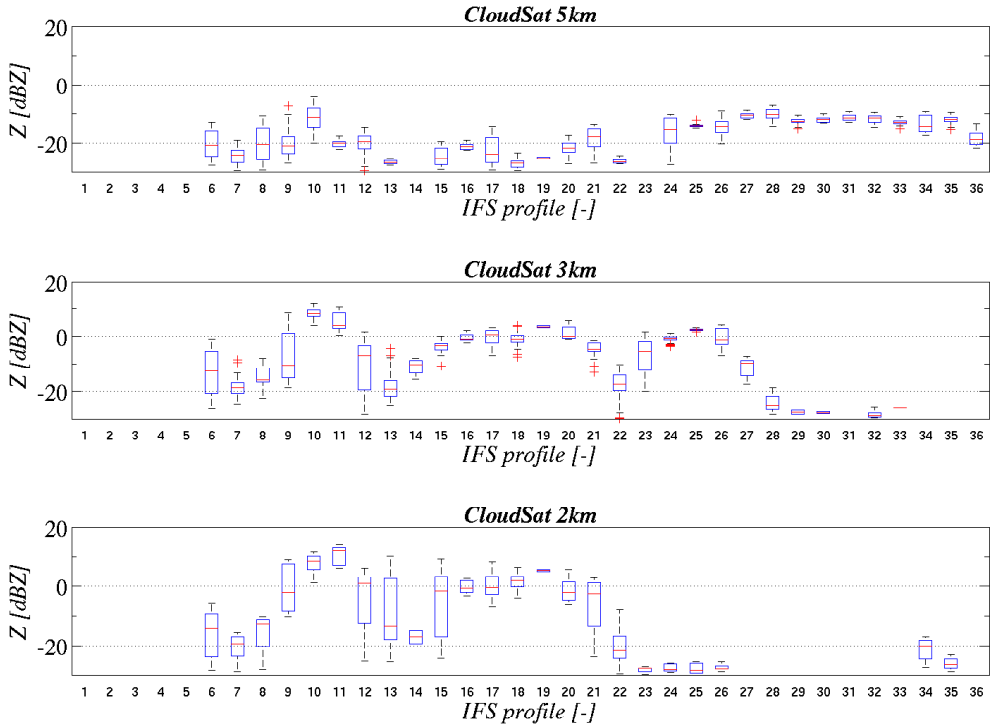

Figure 3.1: *Distribution, shown as box-plot diagram, of the CloudSat reflectivities contained in co-located model grid box. Data refers to the case shown in Fig. 2.2. From top to bottom, panels refer to height above sea level of 5 km, 3 km, 2 km respectively.*

3.1 Scatter plots

Scatter-plots of observations vs. simulations are plotted in Fig. 3.2 considering six reference altitudes.

Fig. 3.2 shows that around 2 km (panel a)) most of the cases have reflectivities between 0 and 10 dBZ. In this range, there is a good correlation between observations and simulations. However, the latter present a small bias of few dBZ. For reflectivities below 0 dBZ, the same plot shows that simulated values are usually larger, especially when observations are below -15 dBZ. This behaviour can be seen also in the observed and simulated reflectivity histograms, plotted along the axes in Fig. 3.2. CloudSat reflectivities show a much wider range of variation, and therefore a broader distribution, while the simulated ones have a well defined peak around 5 dBZ.

At 4 km (panel b) of Fig. 3.2) the comparison appears similar, the main difference being that most of the points lie between 0 and 10 dBZ. When considering reflectivities around 6 km (panel c) of Fig. 3.2), CloudSat reflectivities are usually lower than 0 dBZ and the tendency of ZmVar to overestimate becomes the main feature.

Moving further up to 8 km, 10 km, and 12 km (panels d), e), f) of Fig. 3.2) we note that reflectivities get lower and that the simulated ones tend to group around -20 dBZ, -10 dBZ, and 2 dBZ. These values can be associated to the three ice categories that the ECMWF model prescribes, namely cloud ice, large scale precipitating ice and convective precipitating ice. The behaviour of simulated reflectivities highlights that these three classes can only partially represent the real variability of cloud ice. As a matter of fact, it could be shown that the main features of these plots remain unchanged when using a different parameterization of the ice optical properties.

It is also important to note that similar scatter plots are obtained when the comparison is done using the grid-box mean CloudSat reflectivities (instead of the single shots). It could be shown that the averaging process is only able to increase the agreement for those cases where observations and simulations are very different.

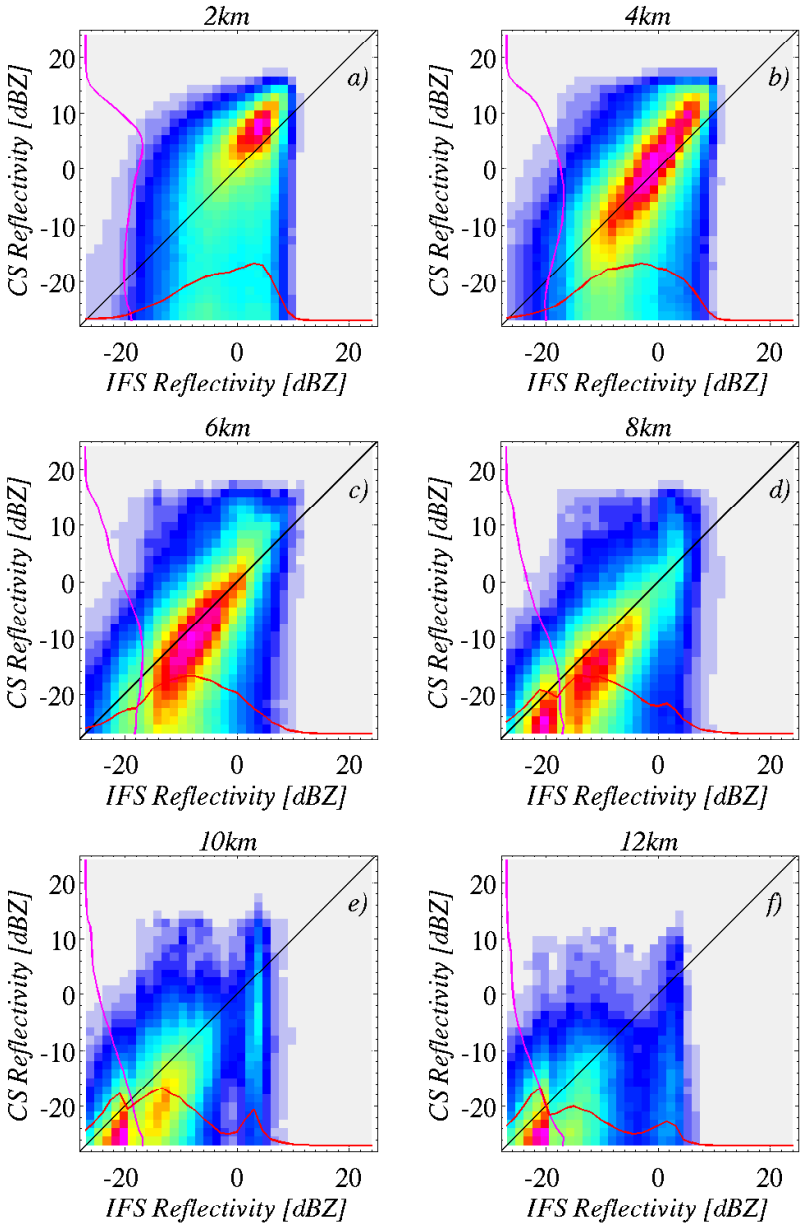

Figure 3.2: *Scatter plot between simulated (on abscissa) and CloudSat reflectivity (on ordinate) using over-ocean matched model-observations relative to 1-20 June 2008. Curves along axes show the relative occurrence of reflectivity values. Each plot refers to the altitude level indicated in the panel title.*

4 First guess departures

Model reflectivities shown in the previous section have been generated mimicking the approach used to define the first guess (FG) of every observation to be assimilated in the operational analysis. In a context of data assimilation, we can therefore think of them as a first guess (FG) for CloudSat observations and we can evaluate the relative departures (defined as observation-minus-FG). In this section, we will investigate how CloudSat FG departures vary in space using the same dataset of 20 days.

In the previous section, scatter plots have shown that simulated reflectivities can be very far from CloudSat observations. In every assimilation system, cases where the first guess is too far from the actual observation are screened out by means of a quality control. This process guarantees, among others, that the linearity hypothesis, needed for the assimilation, is verified. In the following analysis, as condition for quality control we rejected those cases where the FG departures are larger that 9 dBZ.

4.1 Histograms

An illustrative way to show the behaviour of FG departures is by means of cumulative function altitude displays (CFADs), shown in Fig. 4.1. This plot gives, as a function of altitude, the relative occurrence of CloudSat reflectivity FG departures. Departures mean (solid line) and mean±1 standard deviation (dashed lines) are also plotted. In the upper portion of the cloud we note that negative (i.e. FG larger than observations) departures are more frequent. We also note that their amplitude tends to decrease as altitude decreases. Positive FG departures become more frequent between 2 km and 4 km. Below 2 km, large (more than 5 dBZ) either positive or negative departures occur frequently, resulting in an overall small mean value. The negative departures in the upper cloud portions can be explained by the difficulty that every model has to represent the spatial gradients of cloud fields: as shown in Fig. 2.2, simulations tend to produce smoother structures than the actual ones.

First guesses being smaller than observations between 2 km and 4 km is consistent with Fig. 3.2 (panels a) and b)). In fact, at these levels those CloudSat observations with FG departures within the ± 9 dBZ limit have values often above 5 dBZ. We note that in this range simulated reflectivities are systematically larger than observations of few dBZ.

4.2 Geographical distribution

The geographical dependence of CloudSat reflectivity departures has been first investigated considering the variation with latitude. Mean, standard deviation of reflectivity departures, together with number of local observations have been evaluated from our study period over latitude bands and are shown in Fig. 4.2. The mean departures (top panel) exhibit a pattern where the sign varies with height consistently with the CFAD shown above. Interestingly, we note that the height at which the change of sign occurs is latitude dependent. We also note that the negative mean departures between 2 km height and the surface only occur in the Tropical and sub-Tropical regions. Departure standard deviations (middle panel) have little variation with latitude, being slightly larger where higher values of reflectivity are expected, i.e. at lower altitudes (precipitation) and in the Tropics. The number of observations (bottom panel of Fig. 4.2) have a quite uneven distribution across latitudes because only cases over ocean have been considered. This choice, together with the one of June (Austral winter) as study period, explains the much larger number of observations at high latitudes in the Southern hemisphere. It could be shown that observations in the Tropics are also much smaller because many were rejected by the quality control on the amplitude of the departure.

The possible presence of some more regional patterns has been also investigated. Results are plotted in

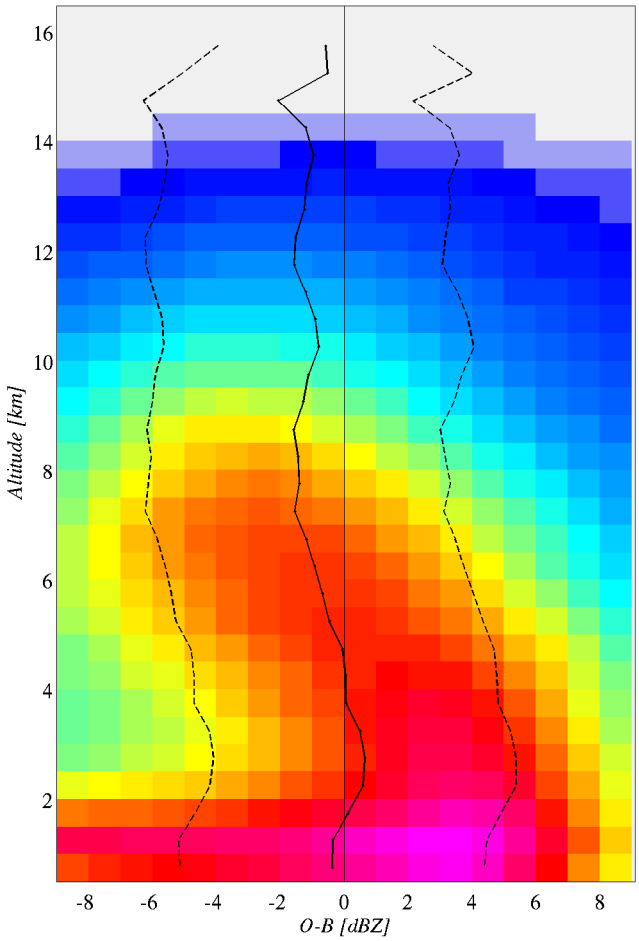

Figure 4.1: *Frequency of occurrence of CloudSat minus first guess reflectivity as function of height above sea level. Over-ocean cases relative to 1-20 June 2008 have been used.*

Figs. 4.3 to 4.5, where quantities in each map are evaluated within boxes having a horizontal extent of 5°by 7.5°(latitude by longitude). Mean FG departures at 6 km (Fig. 4.3, top panel) are negative everywhere at mid and high latitudes, while both positive and negative areas are present in the Tropics. Moving down to 4 km (mid panel), positive patterns tend to dominate in the Tropics and mid latitudes. Mean FG departures at 2 km (bottom panel) became negative in the Tropics, while at mid and high latitudes they are now usually positive with few pockets of negative values.

Standard deviations of FG departure (Fig. 4.4) decrease moving away from the Equator and with altitude, but they don't show any particular features along longitudes. The spatial distribution of CloudSat observations is given in Fig. 4.5. Observations over land are missing because they have been excluded from our analysis. At 2 km (bottom panel) we note that observations cover the entire globe, with the largest number at high latitudes in the Southern Hemisphere (winter).

The number of observations is usually above few hundreds, reaching more than two thousand per grid box in places. At 4 km (mid panel), their number increases in the Northern Hemisphere, while there are no observations in the stratocumulus regions. As expected, at 6 km, the number increases in the Tropics while it decreases at mid latitudes.

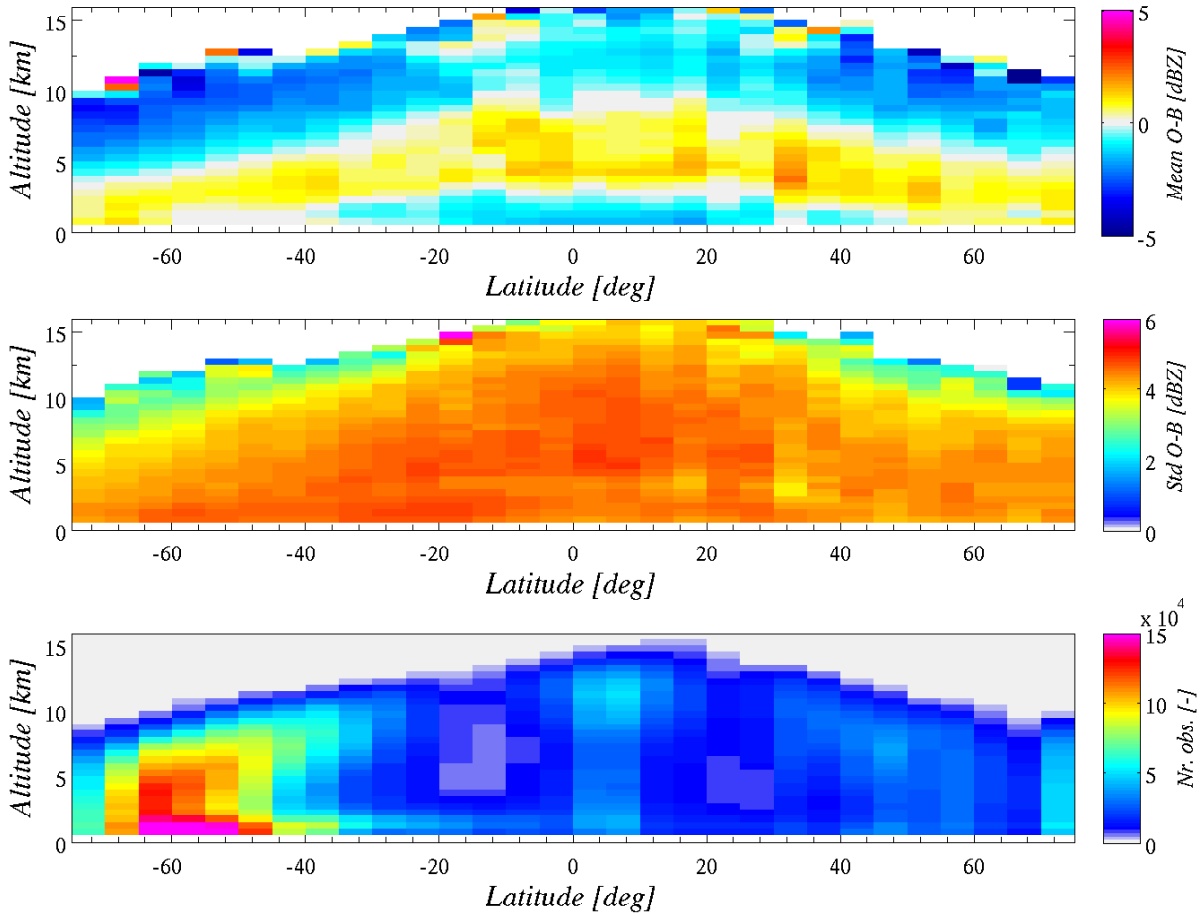

Figure 4.2: *Zonal mean (top panel) and standard deviation (mid panel) of CloudSat first guess departures. The bottom panel gives the number of observations used for their evaluation.*

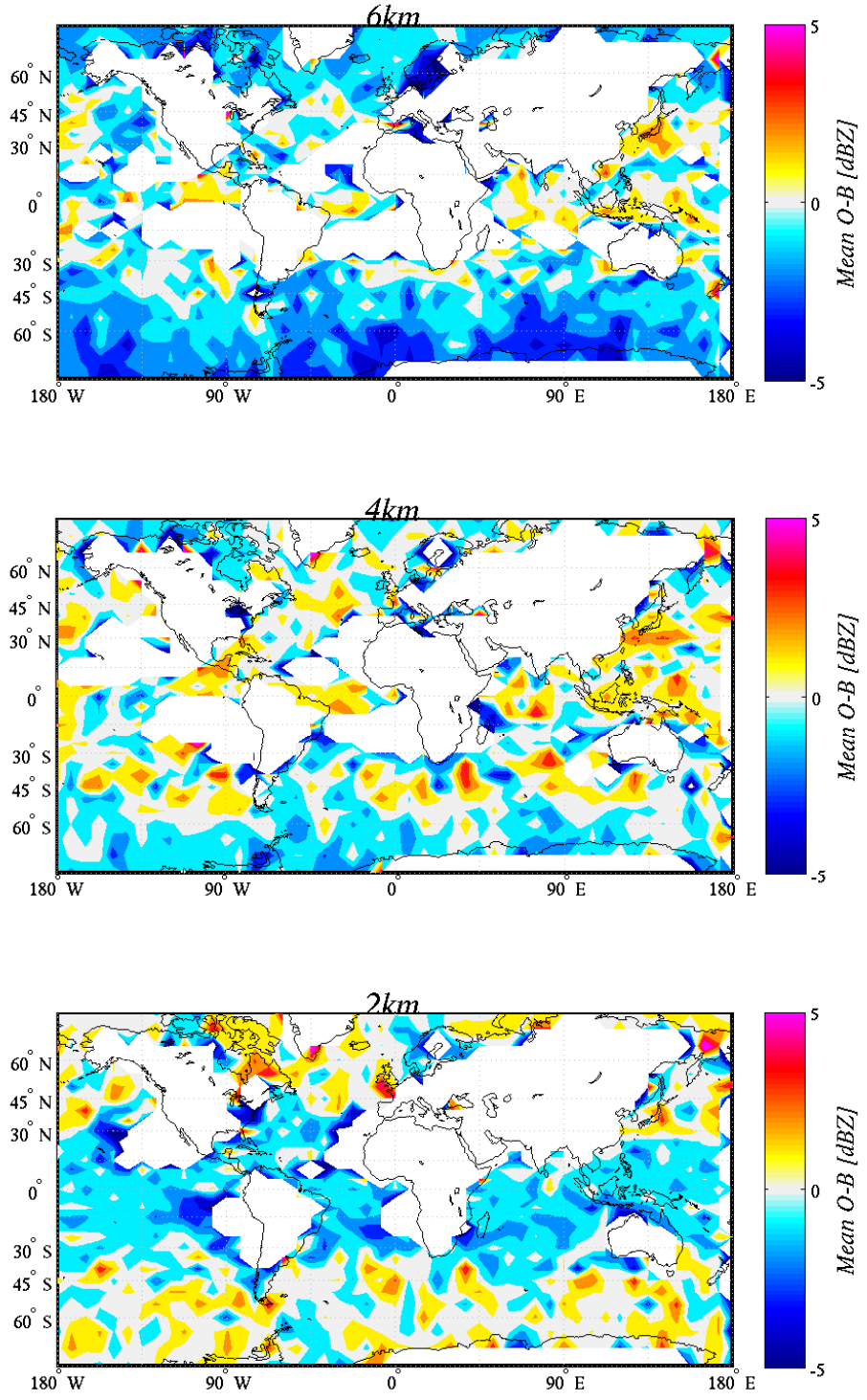

Figure 4.3: *Map of CloudSat reflectivity mean first guess departures at heights of 6 km (top panel), 4 km (mid panel) and 2 km (bottom panel).*

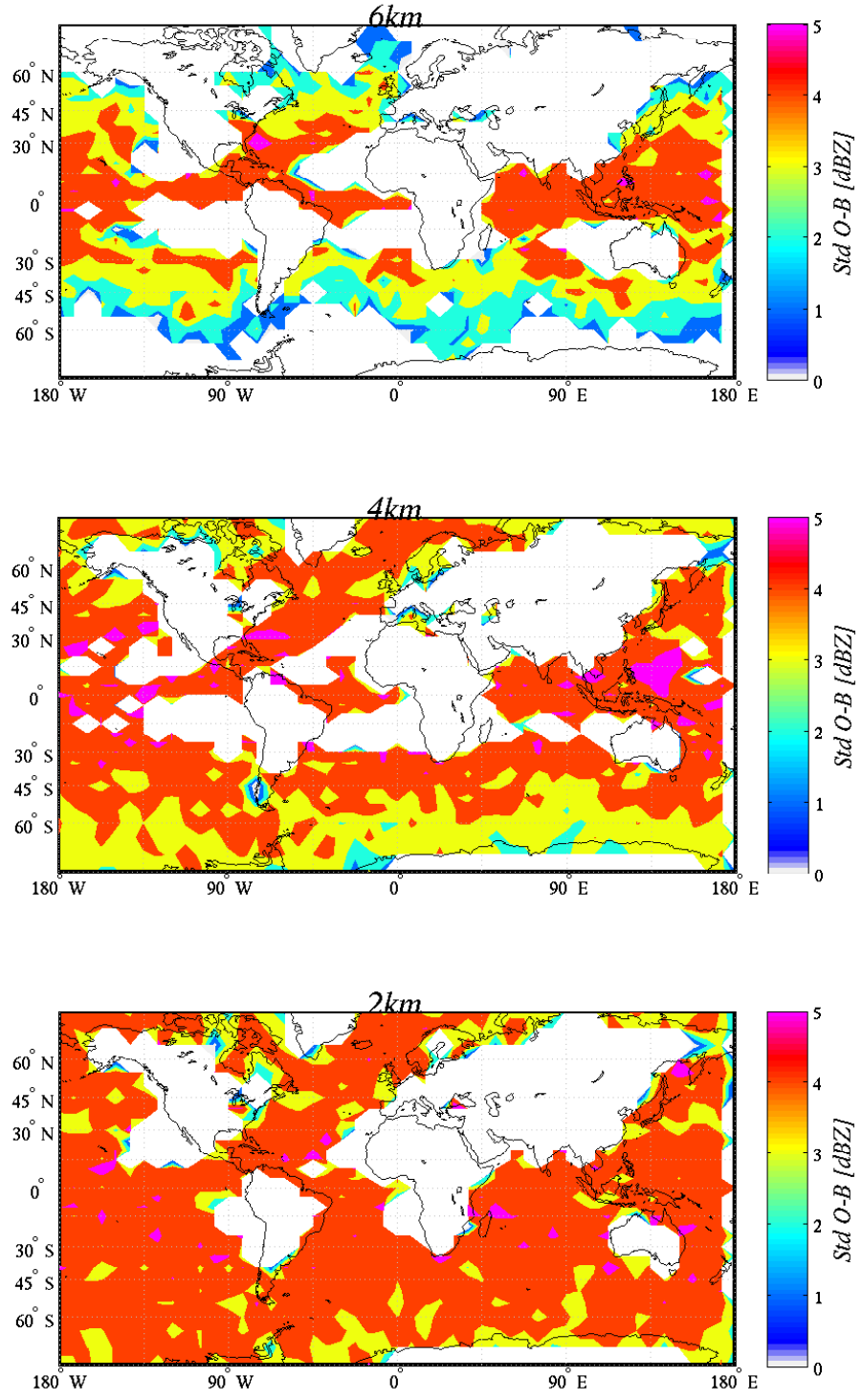

Figure 4.4: *As Fig. 4.3, but showing standard deviation.*

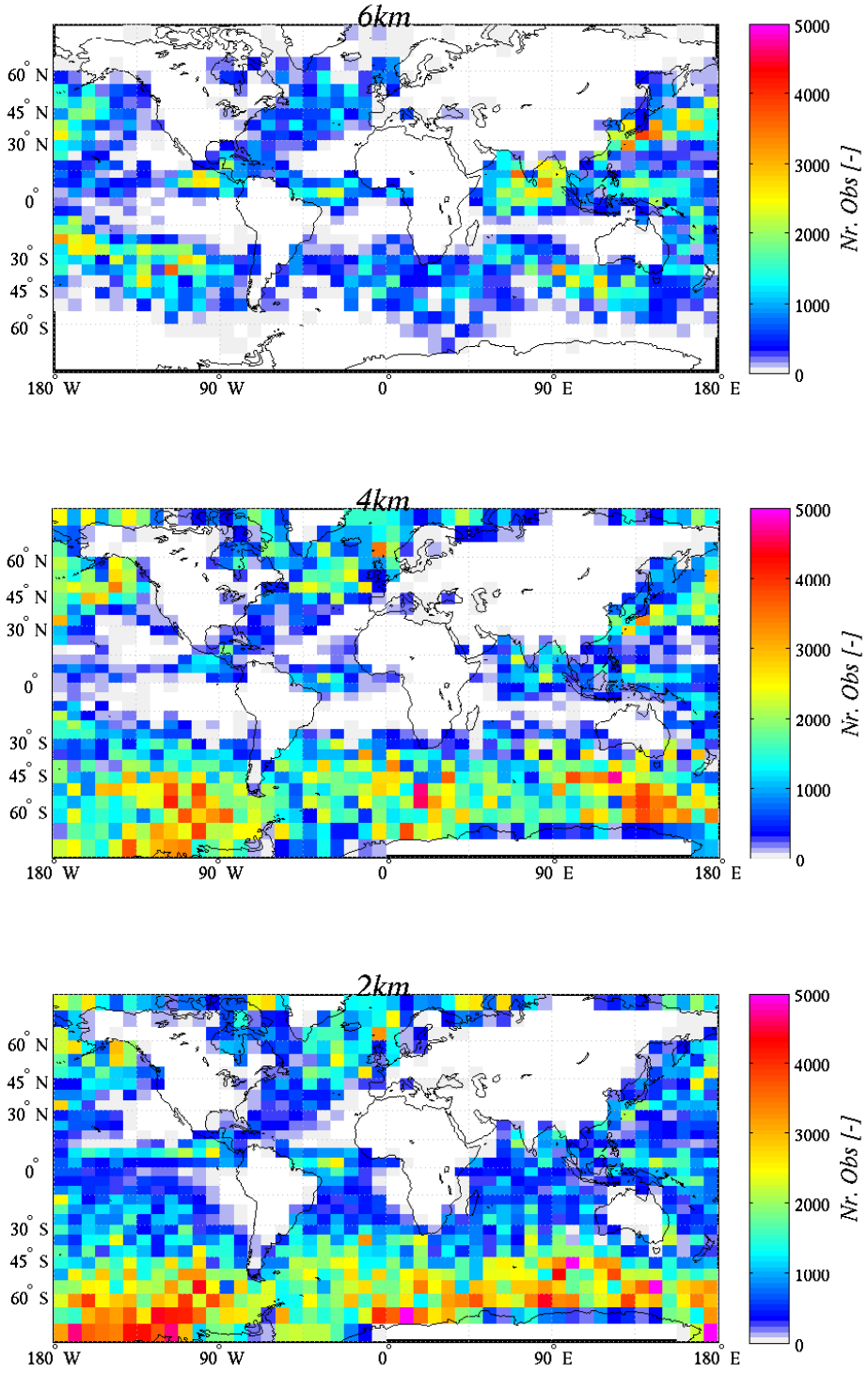

Figure 4.5: *As Fig. 4.3, but showing the number of samples contained into each averaging box.*

5 Monitoring

The temporal evolution of FG (and analysis) departures of each observation type is routinely monitored within the ECMWF assimilation system. In this section, in a similar fashion, time series of CloudSat reflectivity FG departures are evaluated along the 20-day study period. These trends will be used to investigate the possibility of identifying problems with CloudSat data.

5.1 Time series

Temporal trends of FG departures can highlight how differences between model and observations evolve due to changes of the quality of data and/or changes of the forecast model. In this study, as done in the 4D-Var assimilation at ECMWF, time series of CloudSat FG departures have been calculated grouping data within our study period into 12-hour time slots. Mean, standard deviation and number of used FG samples are given respectively in Fig. 5.1 to 5.3, considering high latitudes South (60°S-90°S), mid latitudes South (30°S-60°S) and Tropics (30°S-30°N), separately. Fig. 5.1 shows the time series of mean departures. The most important feature is that the mean is quite stable in time, but we also note that the vertical structure is consistent with the latitude diagram shown in Fig. 4.2. Mean departures are negative above a certain altitude (which is different in the three regions) and positive below. In the Tropics we also find a second negative two-kilometre deep bottom layer. FG standard deviations (Fig. 5.2) do not vary very much in time, too. Again, larger values are found in the Tropics, where reflectivities are likely to be larger. Interestingly, the number of observations for each 12-hour window (Fig. 5.3) can change very rapidly. We note that at high latitudes this number is regular along the vertical, while at mid latitudes and in the Tropics the largest numbers are usually below 2 km.

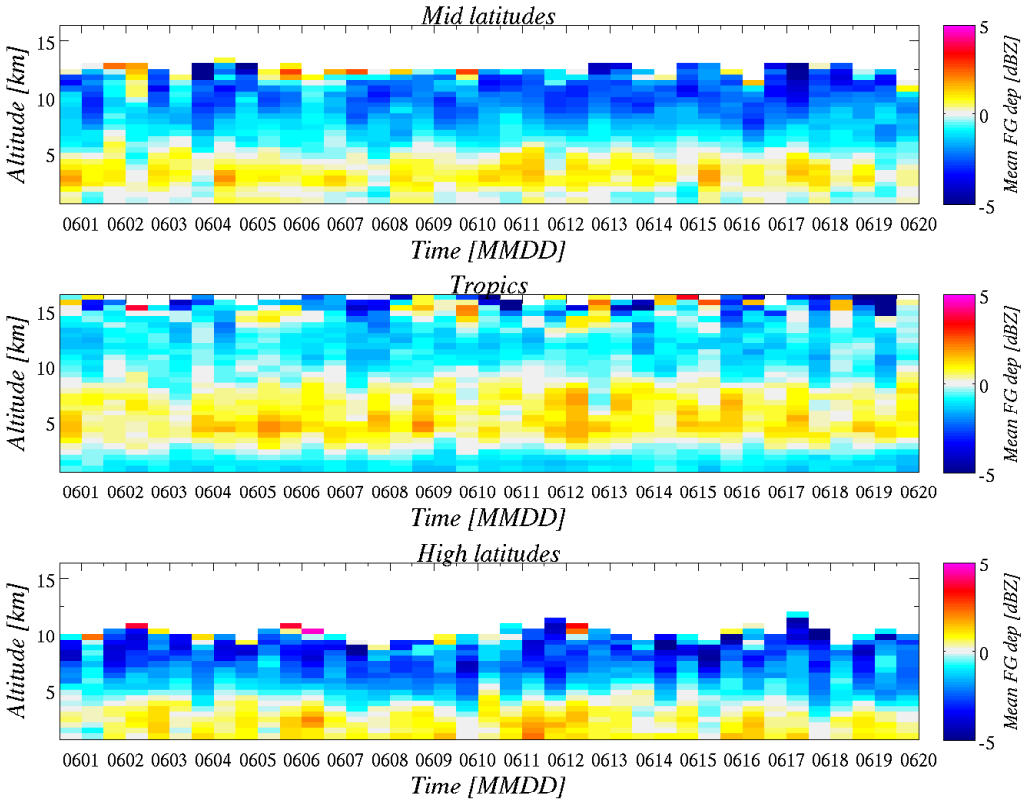

Figure 5.1: *Time series over 12 hours slots of mean first guess departures for CloudSat reflectivity between 1st and 20th of June 2008. From top to bottom: mid latitudes south (30S-60S), Tropics (30S-30N), high latitudes south (below 60S).*

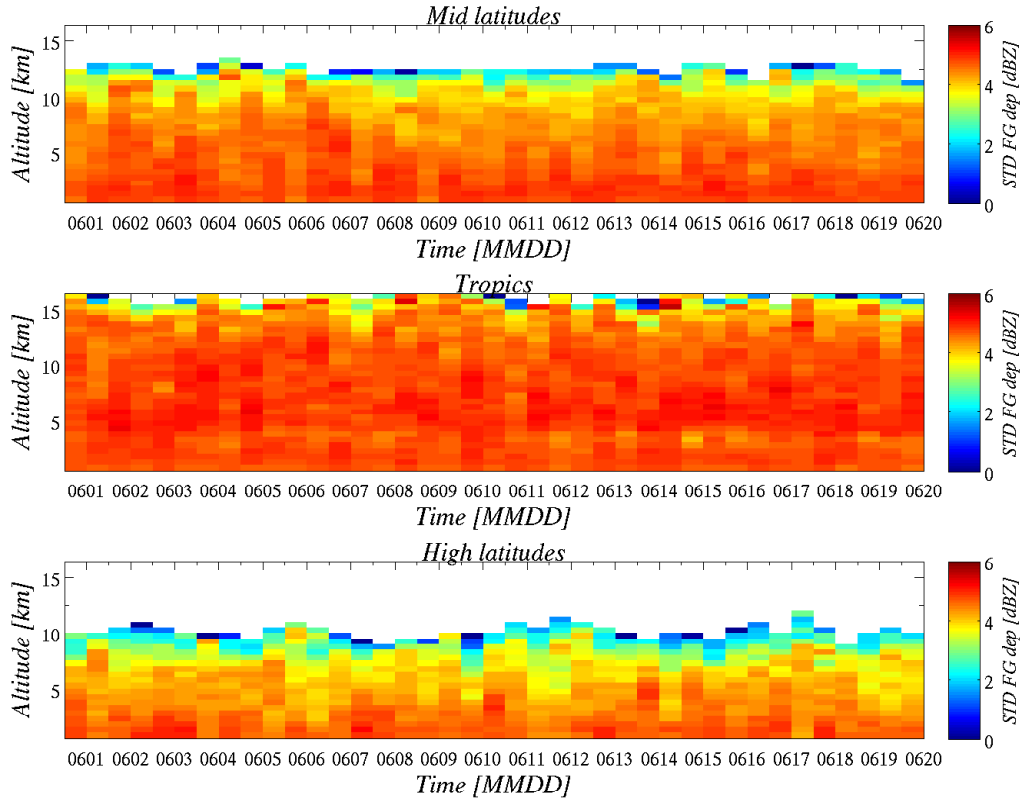

Figure 5.2: *As Fig. 5.1, but plotting standard deviation of first guess departures.*

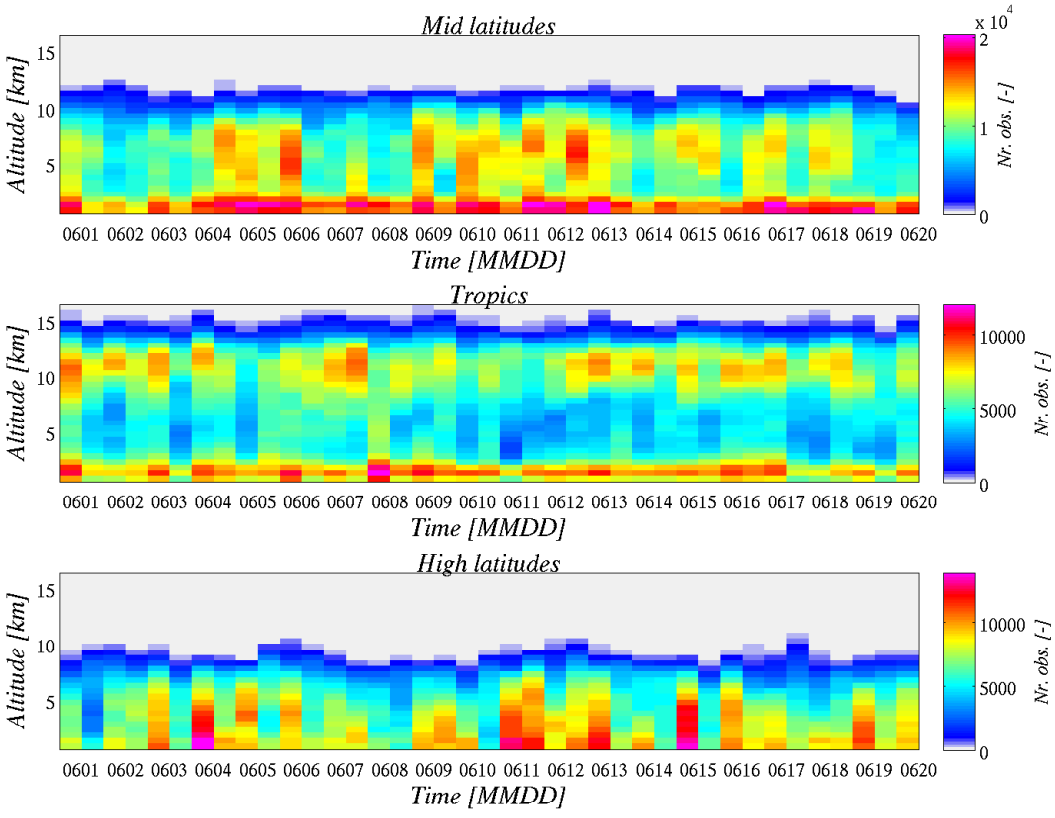

Figure 5.3: *As Fig. 5.1, but plotting the number of samples.*

5.2 Simulation of glitches

As shown in the previous section, statistics of CloudSat reflectivity departures are quite consistent in time. In principle, this feature would be beneficial for recognizing problems with the observations through the identification of situations where departures are outside the normal range of variability. In order to show if this is the case, we have set up two simple experiments where CloudSat observations have been artificially altered to simulate a glitch in the radar measurements.

For this purpose, random noise having Gaussian distribution has been added (in dB units) to the measured CloudSat reflectivities considering two very different forms. The first wants to simulate an instrument calibration issue and therefore has a large (5 dBZ-negative) mean and a small (1 dBZ) standard deviation (Fig. 5.4, red curve). The second wants to represent a partial instrument failure, so it is unbiased but with a large (5 dBZ) standard deviation (Fig. 5.4, blue curve). The chosen numbers for the amplitude of these noises are arbitrary, but they serve the purpose of illustrating the concept.

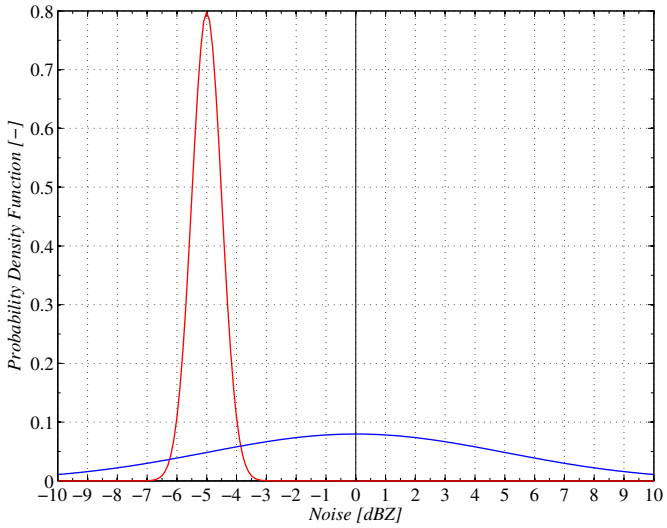

Figure 5.4: *Probability density function of the two random noises used to perturb CloudSat observations.*

Each of these expressions has been applied separately to CloudSat data over 5 consecutive days starting on day-11 of the study period. The effect on the departure time series is shown in Fig. 5.5, Fig. 5.6 and Fig. 5.7 for reflectivities at mid latitudes around 3 km, 6 km and 9 km, respectively.

The mean departure (top panels) for the biased noise (red curve) shows a clear drop during the failure period, while in case of unbiased noise (blue curve) the change is smaller than the typical oscillations. As expected, it would be therefore difficult to reveal an unbiased noise, although quite large, along a time series of mean departures.

Departure standard deviations (mid panels) increase in the case of noise with strong variance (blue curve). Instead, when the biased noise (red curve) is applied, we see a reduction in the standard deviation of departures. It could be shown that this behaviour is consequence of a distribution of FG departures which is narrower in case of because 'pushed' toward the lower limit of -9 dBZ by the strong biased noise.

Fig. 5.5 to Fig. 5.7 show that the number of observations (bottom panels) always decreases because when noise is added more cases fall outside the limit set for the maximum allowed departure ($\pm$9 dBZ).

These examples show that unexpected glitches of reflectivity measurements can be identified if they lead to appreciable changes in the time trends of FG departures. The routine monitoring of mean and standard

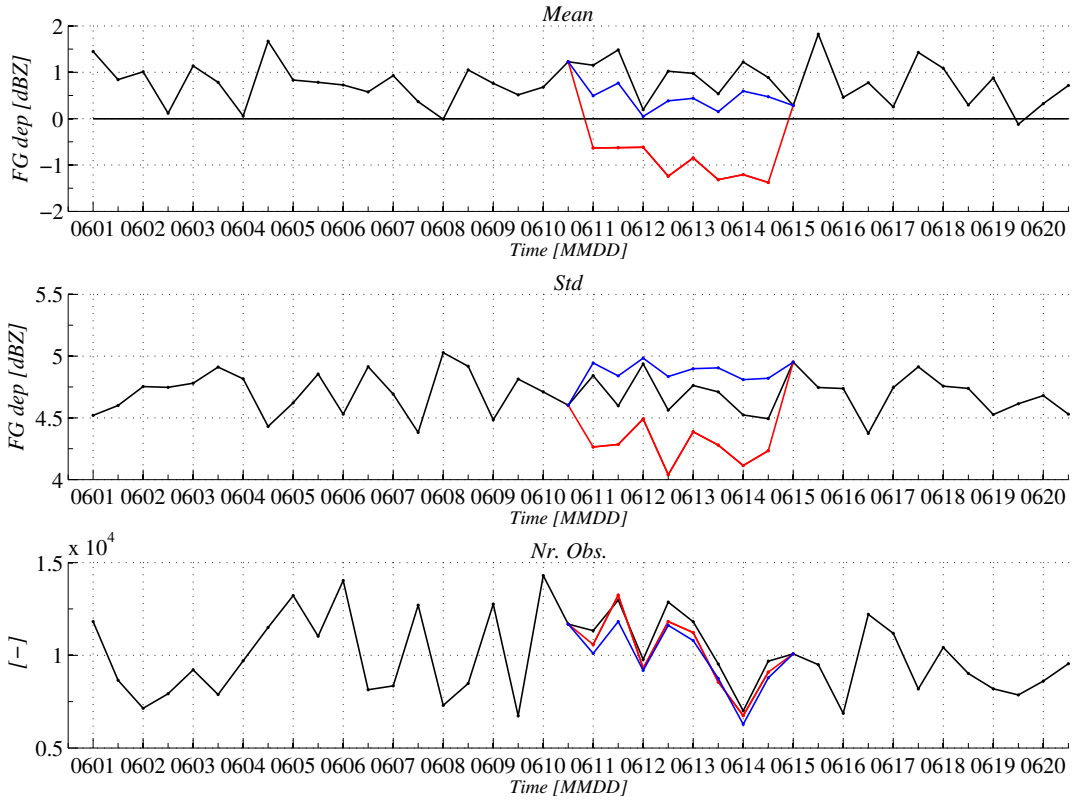

Figure 5.5: *Time series of first guess departures for CloudSat reflectivity between 1st and 20th of June 2008. Only observations at around 3 km and at mid latitudes South (30S-60S) are considered. From top to bottom: mean, standard deviation and number of samples. Black lines refer to the case with untouched CloudSat measurements, while blue and red are relative to the experiments where CloudSat measurements are perturbed with one of the random noises shown in Fig. 5.4.*

deviation of reflectivity FG departures coupled with an ad hoc system of threshold values should makes possible the identification of such anomalies.

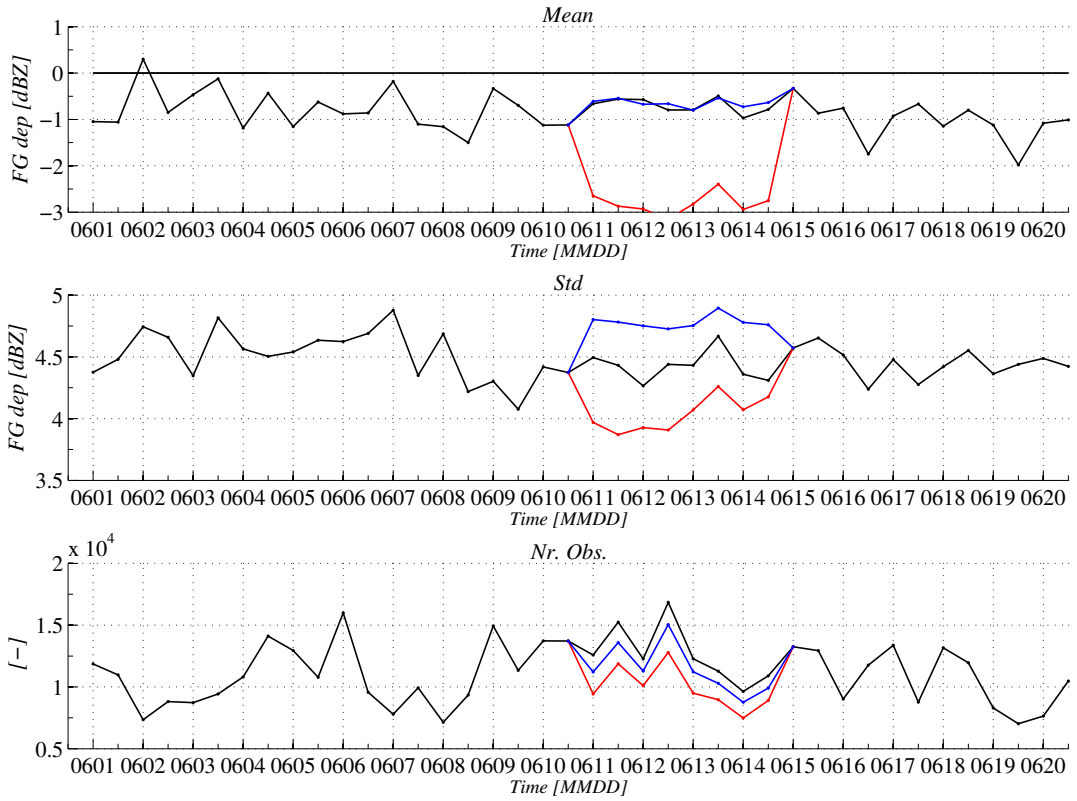

Figure 5.6: *As Fig. 5.5, but for reflectivity around 6 km.*

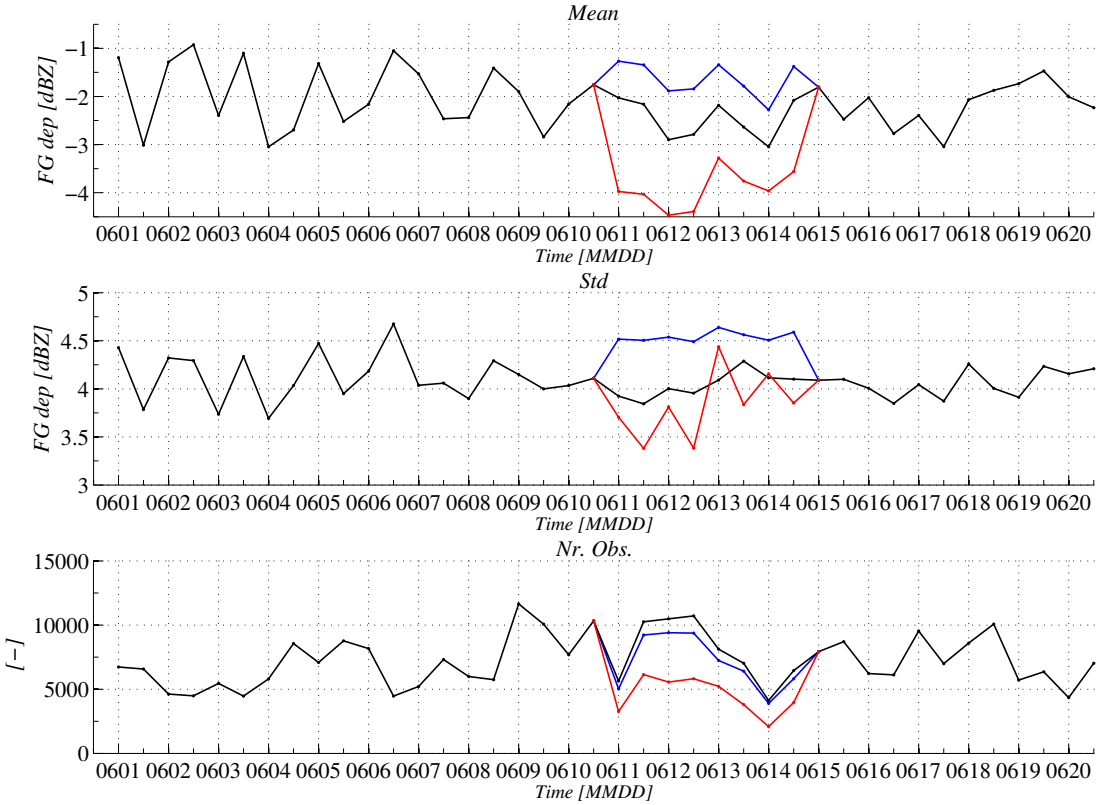

Figure 5.7: *As Fig. 5.5, but for reflectivity around 9 km.*

6 Summary and conclusions

In this study, a monitoring system for CloudSat observations has been put in place. The procedure consists of a series of tasks to be executed off-line of the full ECMWF assimilation system. As a first step, short-term forecasts of the ECMWF model are run and those variables needed for the ZmVar forward operator are saved. In a second step, those profiles closest to CloudSat observations are then selected among the global fields. ZmVar is then run on these profiles and a FG of CloudSat reflectivity can be in this way determined. After this step, the FG departures of CloudSat reflectivity are evaluated. The feasibility of monitoring possible problems with data has been investigated analyzing statistics of FG departures over a 20-day study. We have shown that when CloudSat measurements are deteriorated adding random noise that time series of FG departures can be brought outside their normal range of variation. In these cases, such glitches could be therefore identified by devising an alert system based on threshold levels.

Acknowledgements

The authors are grateful to the NASA CloudSat Project for providing the CloudSat data used in this study.

A List of Acronyms

4D-Var	Four-Dimensional Variational assimilation
CFAD	Cumulative Function Altitude Display
CloudSat	NASA's cloud radar mission
EarthCARE	Earth, Clouds, Aerosols and Radiation Explorer
ECMWF	European Centre for Medium-Range Weather Forecasts
ESA	European Space Agency
FG	First Guess
NASA	National Aeronautics and Space Administration
ZmVar	Z (reflectivity) Model for Variational Assimilation of ECMWF

References

Auligne, T. and A. McNally, 2007: Interaction between bias correction and quality control, *Quarterly Journal of the Royal Meteorological Society*, **133**(624), 643–653.

Di Michele, S., O. Stiller, and R. Forbes, 2009: QuARL WP1000 Report: Forward operator developments - Errors and biases in representativity, Technical report, ECMWF.

Stephens, G., D. Vane, R. Boain, G. Mace, K. Sassen, Z. Wang, A. Illingworth, E. O'Connor, W. Rossow, S. Durden, *et al.*, 2002: The CloudSat mission and the A-Train, *Bulletin of the American Meteorological Society*, **83**(12), 1771–1790.